The Extracellular Zn²⁺ Concentration Surrounding Excited Neurons Is High Enough to Bind Amyloid-β Revealed by a Nanowire Transistor

Ankur Anand, Chih-Hung Chi, Subhasree Banerjee, Ming-Yi Chou, Fan-Gang Tseng, Chien-Yuan Pan,* and Yit-Tsong Chen*

The Zn²⁺ stored in the secretory vesicles of glutamatergic neurons is coreleased with glutamate upon stimulation, resulting in the elevation of extracellular Zn²⁺ concentration ($C_{Zn^{2+}}^{ex}$). This elevation of $C_{Zn^{2+}}^{ex}$ regulates the neurotransmission and facilitates the fibrilization of amyloid-β (Aβ). However, the exact $C_{Zn^{2+}}^{ex}$ surrounding neurons under (patho)physiological conditions is not clear and the connection between $C_{Zn^{2+}}^{ex}$ and the Aβ fibrilization remains obscure. Here, a silicon nanowire field-effect transistor (SiNW-FET) with the Zn²⁺-sensitive fluorophore, FluoZin-3 (FZ-3), to quantify the $C_{Zn^{2+}}^{ex}$ in real time is modified. This FZ-3/SiNW-FET device has a dissociation constant of ≈12×10^{-9} M against Zn²⁺. By placing a coverslip seeded with cultured embryonic cortical neurons atop an FZ-3/SiNW-FET, the $C_{Zn^{2+}}^{ex}$ elevated to ≈110×10^{-9} M upon stimulation with α-amino-3-hydroxy-5-methyl-4-isoxazolepropionic acid (AMPA). Blockers against the AMPA receptor or exocytosis greatly suppress this elevation, indicating that the Zn²⁺ stored in the synaptic vesicles is the major source responsible for this elevation of $C_{Zn^{2+}}^{ex}$. In addition, a SiNW-FET modified with Aβ could bind Zn²⁺ with a dissociation constant of ≈633×10^{-9} M and respond to the Zn²⁺ released from AMPA-stimulated neurons. Therefore, the $C_{Zn^{2+}}^{ex}$ can reach a level high enough to bind Aβ and the Zn²⁺ homeostasis can be a therapeutic strategy to prevent neurodegeneration.

1. Introduction

The homeostasis of Zn²⁺ in the cytosol and extracellular matrix is important for various biological activities, such as apoptosis,[1] DNA synthesis,[2] enzyme activities,[3] gene expression,[4] immune system function,[5] and neurotransmission.[6] The free intracellular Zn²⁺ concentration ($C_{Zn^{2+}}^{in}$) is maintained at a sub-nanomolar (<10^{-9} M) level by three main mechanisms. The first is chelation by abundant metallothioneins with their seven Zn²⁺-binding sites; the second and third mechanisms are the Zn²⁺ transporters (ZnTs) and the Zrt/Irt-like proteins (ZIPs) that flux Zn²⁺ in and out of the cytosol, respectively, across the membranes of cells and intracellular organelles.[7] Extracellularly, abundant Zn²⁺-binding proteins sequester Zn²⁺ to lower the Zn²⁺ concentration ($C_{Zn^{2+}}^{ex}$) to a nanomolar (nM) level at the resting state.[8,9] To date, Zn²⁺ dyshomeostasis has been reported to implicate neurodegenerative disorders, such as Alzheimer's and Parkinson's diseases.[10–13]

The ZnT-3 proteins on the synaptic vesicles of glutamatergic neurons fill the interiors of vesicles with high $C_{Zn^{2+}}$ of $100–300 \times 10^{-6}$ M, which is coreleased with glutamate upon stimulation of exocytosis.[14,15] The synaptically released Zn²⁺ interacts with various ion channels, receptors, and transporters, modulating synaptic plasticity.[6] In cultured neocortical and hippocampal neurons, Zn²⁺ at the nanomolar

A. Anand, Prof. F.-G. Tseng
Department of Engineering and System Science
National Tsing Hua University
Hsinchu 30013, Taiwan
A. Anand
Nanoscience and Technology Program
Taiwan International Graduate Program
Academia Sinica
Taipei 115, Taiwan
A. Anand, Dr. S. Banerjee, Prof. Y.-T. Chen
Institute of Atomic and Molecular Sciences
Academia Sinica
Taipei 106, Taiwan
E-mail: ytcchem@ntu.edu.tw

The ORCID identification number(s) for the author(s) of this article can be found under https://doi.org/10.1002/smll.201704439.

Prof. F.-G. Tseng
Frontier Research Center on Fundamental
and Applied Sciences of Matters
National Tsing Hua University
Hsinchu 30013, Taiwan
Prof. F.-G. Tseng
Research Center for Applied Sciences
Academia Sinica
Taipei 115, Taiwan
Dr. C.-H. Chi, Dr. S. Banerjee, Dr. M.-Y. Chou, Prof. C.-Y. Pan
Department of Life Science
National Taiwan University
Taipei 106, Taiwan
E-mail: cypan@ntu.edu.tw
Dr. S. Banerjee, Prof. Y.-T. Chen
Department of Chemistry
National Taiwan University
Taipei 106, Taiwan

level attenuates the activities of both *N*-methyl-D-aspartate (NMDA) and γ-aminobutyric acid type A receptors but mildly potentiates the excitation mediated by the α-amino-3-hydroxy-5-methyl-4-isoxazolepropionic acid (AMPA) receptor (referred to as AMPAR hereafter), thereby influencing both excitatory and inhibitory synaptic transmissions in the brain.[16,17] Over the years, many studies have been conducted to elucidate the transient $C_{Zn^{2+}}^{ex}$ surrounding the neurons during excitation, but the exact $C_{Zn^{2+}}^{ex}$ is controversial, with a range of $1–100 \times 10^{-6}$ M.[18–20] Moreover, some studies have even suggested that the elevated $C_{Zn^{2+}}^{ex}$ is below micromolar (μM) levels.[21–23]

The accumulation of extracellular Zn^{2+} can lead to neuronal death via processes such as autophagy activation,[24] mitochondrial dysfunction,[25] and protein aggregation.[26] Since the $C_{Zn^{2+}}$ in a synaptic vesicle is over several hundred μM, it is usually assumed that the elevated $C_{Zn^{2+}}^{ex}$ is at the same level, which has been adopted by many studies on the effects of Zn^{2+}-related toxicity in neurons.[27] However, the abundant Zn^{2+}-binding proteins in the extracellular space maintain the $C_{Zn^{2+}}^{ex}$ at a low level, but the exact free $C_{Zn^{2+}}^{ex}$ has not been settled.[18,28] The exposure of cultured cortical neurons to different levels of $C_{Zn^{2+}}^{ex}$ can cause dose and duration-dependent neuronal injuries.[29] In addition, Zn^{2+} facilitates the aggregation of amyloid-β (Aβ), which is a risk factor responsible for neurodegeneration and Alzheimer's disease;[26] therefore, the prevention of Zn^{2+}-induced Aβ toxicity is a plausible therapeutic strategy.[30] Consequently, these queries arouse our interest to accurately evaluate the toxic effect of elevated $C_{Zn^{2+}}^{ex}$.

Silicon nanowire field-effect transistors (SiNW-FETs)-based biosensors are reliable, sensitive, label-free, and real-time tools that have been widely applied to analyze the release of biological molecules from cells.[31–38] In this report, we modified a multiple parallel-connected SiNW-FET with the Zn^{2+}-sensitive fluorophore of FluoZin-3 (referred to as FZ-3/SiNW-FET) to quantify the Zn^{2+} released from excited neurons in real time. By placing a coverslip seeded with cultured embryonic cortical neurons atop an FZ-3/SiNW-FET, the $C_{Zn^{2+}}^{ex}$ surrounding the excited neurons elevated to $\approx 110 \times 10^{-9}$ M upon the stimulation with AMPA. By adding the blockers against AMPAR, the AMPA-induced excitation greatly suppressed the elevation in $C_{Zn^{2+}}^{ex}$. In addition, a SiNW-FET modified with Aβ (Aβ/SiNW-FET) could bind Zn^{2+} with dissociation constant (K_d) of $\approx 633 \times 10^{-9}$ M and respond to the Zn^{2+} released from AMPA-stimulated neurons. Consequently, the free $C_{Zn^{2+}}^{ex}$ surrounding the excited neurons is high enough to bind Aβ and the $C_{Zn^{2+}}^{ex}$ homeostasis is important for the health of the brain.

2. Results and Discussions

To detect the Zn^{2+} released from neurons, we placed a coverslip seeded with cortical neurons atop an FZ-3/SiNW-FET with the neurons facing the sensing device, as illustrated schematically in **Figure 1**a. A SiNW-FET chip comprises six sensing devices (Figure S1a, Supporting Information), where each device consists of several tens of p-type single-crystalline boron-doped SiNWs (≈ 20 nm in diameter each) entrapped beneath a set of interdigitated source–drain electrodes (Figure 1b). Figure 1c shows a bright-field image of the cultured cortical neurons. To

characterize the electrical properties of the SiNW-FET device in ambient conditions (Figure S1b, Supporting Information), we first applied a ramp voltage from -200 to $+200$ mV between the interdigitated source and drain electrodes (V_{sd}), where the linear profile of the corresponding current (I_{sd}) indicated an ohmic contact of the electronic device. Then, we immersed the SiNW-FET device in HEPES buffer (50×10^{-3} M of 4-(2-hydroxyethyl)-1-piperazineethanesulfonic acid, pH 7.4), set the V_{sd} at $+10$ mV, and applied a ramp voltage through a solution-gate electrode (V_g) (Figure 1a). For a p-type SiNW-FET, the measured $I_{sd}–V_g$ curve provided an electrical transconductance of ≈ 900 nS (Figure S1c, Supporting Information). These results indicate that the SiNW-FET device has high-performance output ($I_{sd}–V_{sd}$) and transfer ($I_{sd}–V_g$) characteristics.

FZ-3 is a specific Zn^{2+}-sensitive fluorophore with a K_d of $\approx 15 \times 10^{-9}$ M for the Zn^{2+}-FZ-3 complex.[39,40] To make a SiNW-FET with Zn^{2+}-detecting capability, we immobilized FZ-3 to a 3-chloropropyltrimethoxysilane-modified SiNW-FET (CPTMS/SiNW-FET, Figure 1d) with the chemical procedures illustrated in Figure S2 (Supporting Information) and described in the Experimental Section. In the presence of Zn^{2+} (1×10^{-6} M), the uniform fluorescence of the FZ-3-immobilized SiO_2/Si substrate (Figure S3a, Supporting Information) confirmed the homogeneous distribution of the FZ-3 on the SiO_2/Si surface. In addition, the emission spectra of the immobilized FZ-3 and the Zn^{2+}-FZ-3 complex in solution were alike,[39] indicating that the immobilized FZ-3 still maintained the chelation ability against Zn^{2+}. The observed $I_{sd}–V_g$ curves of the FZ-3/SiNW-FET (Figure S3d, Supporting Information) shifted downward in the presence of Zn^{2+}, indicating the positive gating of Zn^{2+} to the p-type FZ-3/SiNW-FET and demonstrating the successful detection of Zn^{2+} by FZ-3/SiNW-FET.

To determine the sensitivity of FZ-3/SiNW-FET against Zn^{2+}, we perfused the FZ-3/SiNW-FET device with different $C_{Zn^{2+}}$ through a polydimethylsiloxane (PDMS) microfluidic channel. **Figure 2**a shows that the measured $I_{sd}–V_g$ curves shifted downward as the $C_{Zn^{2+}}$ increased from 100×10^{-15} to 8×10^{-6} M. To avoid device-to-device variation, we converted the current change caused by receptor-target binding (ΔI_{sd} at $V_g = 0$ V, relative to the buffer solution) to the corresponding change in V_g (ΔV_g^{cal}, termed the "calibrated response") from the transfer curves ($I_{sd}–V_g$) of the FET device used (Figure S4, Supporting Information).[37,41] As plotted in Figure 2b, the normalized response ($\Delta V_{g,Zn^{2+}}^{cal}/\Delta V_{g,Zn^{2+}}^{cal,max}$) increased as the $C_{Zn^{2+}}$ rose, which then reached a plateau at $C_{Zn^{2+}} > 2 \times 10^{-6}$ M (i.e., the saturated $\Delta V_{g,Zn^{2+}}^{cal}$ and denoted by $\Delta V_{g,Zn^{2+}}^{cal,max}$). For the SiNW-FET modified with propyltrimethoxysilane only (referred as trimethoxypropylsilane PTMS/SiNW-FET, a negligible electrical conductance change was observed even in response to the highest concentration (8×10^{-6} M) of $C_{Zn^{2+}}$ (Figure 2c).

To calculate the binding affinity of FZ-3/SiNW-FET against Zn^{2+}, we plotted the $C_{Zn^{2+}}/\Delta V_{g,Zn^{2+}}^{cal}$ versus $C_{Zn^{2+}}$ curve (the inset of Figure 2b), where the $K_d = 12.0 \pm 3.2 \times 10^{-9}$ M of the Zn^{2+}-FZ-3 complex was determined by a least-squares fit to the Langmuir adsorption isotherm model (details in Section S2, Supporting Information). This value is close to the K_d ($\approx 15 \times 10^{-9}$ M) obtained from a fluorescence experiment reported previously.[39] The linear working range of the FZ-3/SiNW-FET spanned from 10^{-11} to 10^{-6} M (the red dots in Figure 2c,d) with a limit of
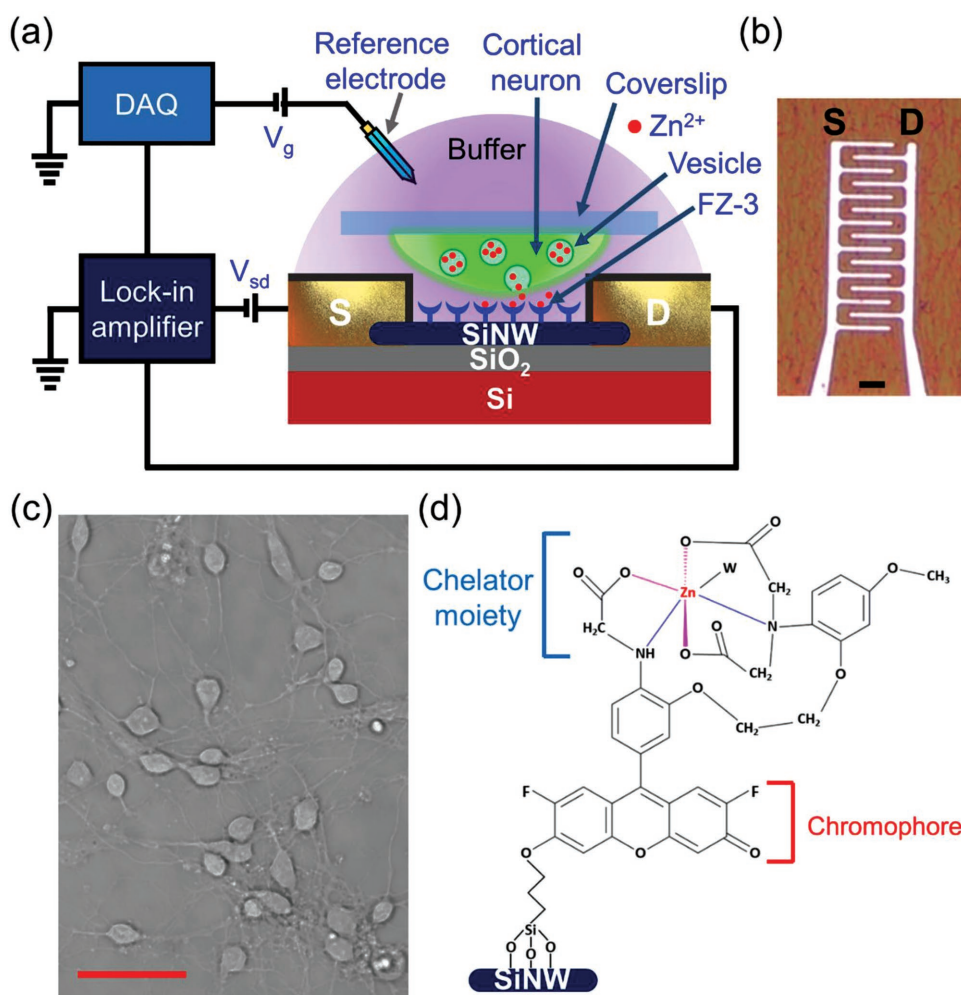
Figure 1. Detection of the Zn^{2+} release from neurons by SiNW-FET. a) Schematic illustration of an FZ-3/SiNW-FET biosensor. The cortical neurons grown on a coverslip were placed in intimate contact with the SiNW-FET modified with a Zn^{2+}-sensitive fluorophore of FZ-3. An Ag/AgCl reference electrode was used as a solution-gate electrode. Upon stimulation, the Zn^{2+} ions released from cortical neurons bind the FZ-3/SiNW-FET, thus inducing the conductance change inside the SiNW-FET. b) An optical microscopy image of a SiNW-FET device. The SiNWs were located underneath and placed between the interdigitated source (S) and drain (D) electrodes. Scale bar: 10 μm. c) A differential interference contrast image of cultured neurons. Scale bar: 50 μm. d) The chemical structures of FZ-3 and the Zn^{2+}-FZ-3 complex.[40] In FZ-3, the two N atoms of the aminocarboxylate moieties and the three O atoms of the carboxyl groups are responsible for the Zn^{2+} binding. A coordinated water molecule in the binding complex is marked by W. The drawings in (a) and (d) are not to scale.

detection of ≈10^{-11} M. By comparison, the fluorescence measurements using FZ-3 could only detect Zn^{2+} in the small range of 10^{-9}–10^{-7} M.[39] In probing Zn^{2+}, the wide linear working range and the low limit of detection make this sensitive FZ-3/SiNW-FET biosensor suitable for detecting minute changes in biological $C_{Zn^{2+}}$.

To characterize the selectivity of the FZ-3/SiNW-FET device toward various biologically relevant ions, we perfused the FZ-3/SiNW-FET device with HEPES buffer containing various ions (Zn^{2+}, Fe^{2+}, Ca^{2+}, Mn^{2+}, and Mg^{2+}) at different concentrations and recorded the conductance responses (Figure 2d). By plotting the normalized $\Delta V^{cal}_{g,Zn^{2+}}/\Delta V^{cal,max}_{g,Zn^{2+}}$ (%) against $C_{M^{2+}}$ (M^{2+} = Fe^{2+}, Ca^{2+}, Mn^{2+}, or Mg^{2+}), the results show that these divalent ions did not cause an appreciable conductance change, except that Fe^{2+} had a slight affinity for FZ-3 ($K_d = 1.1 \pm 0.2 \times 10^{-6}$ M) but was still 100-fold weaker than the Zn^{2+}-FZ-3 binding. It is

worth noting that FZ-3 does not have appreciable binding to monovalent ions, such as Na^+ and K^+;[42] moreover, Ca^{2+} and Mg^{2+} caused little response with the FZ-3/SiNW-FET device even at very high concentration of 2×10^{-3} M (Figure S5, Supporting Information). These results indicate that the FZ-3/SiNW-FET can bind Zn^{2+} specifically and measure the $C_{Zn^{2+}}$ in a biological milieu.

The corelease of Zn^{2+} with glutamate from synaptic vesicles during neurotransmission may elevate the local $C^{ex}_{Zn^{2+}}$, but the exact $C^{ex}_{Zn^{2+}}$ is still controversial. To demonstrate the capability of an FZ-3/SiNW-FET device to detect the Zn^{2+} released from live neurons, we placed a coverslip seeded with cortical neurons (days in vitro 7–14) in intimate contact with the FZ-3/SiNW-FET (Figure 1a). To study the cellular response under a physiological condition, we used balanced salt saline (BSS, in mM, 1.26 $CaCl_2$, 5.33 KCl, 0.5 $MgCl_2$, 0.4 $MgSO_4$, 138 NaCl,

**ADVANCED
SCIENCE NEWS**

www.advancedsciencenews.com

NANO · MICRO

small

www.small-journal.com
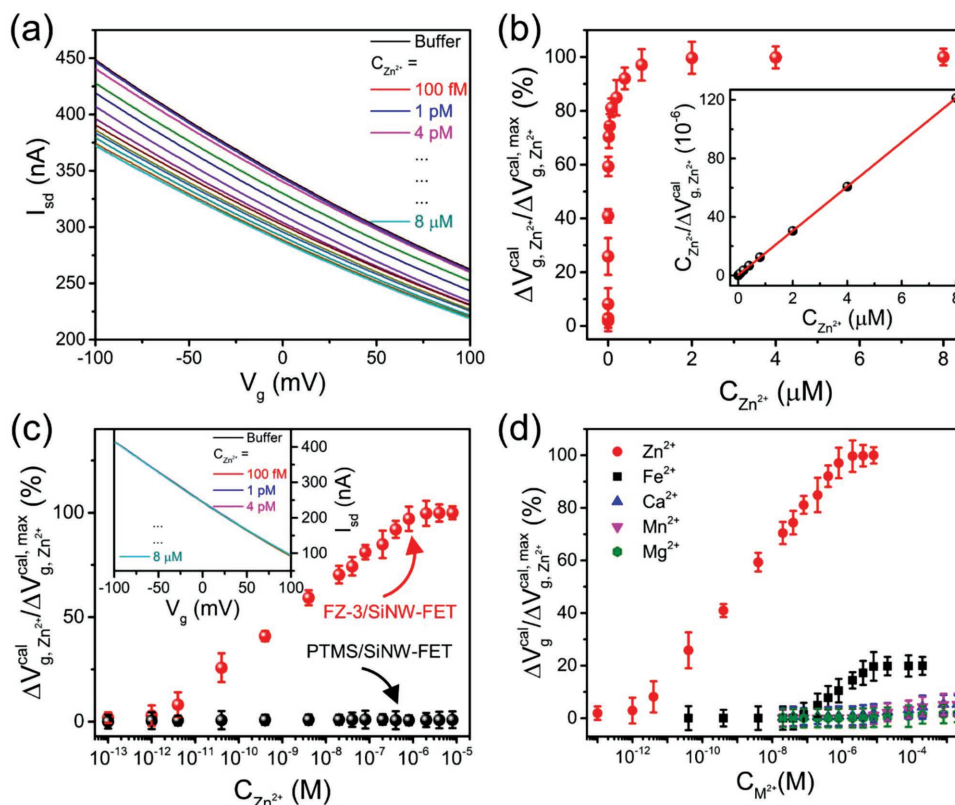
Figure 2. An FZ-3/SiNW-FET captures Zn^{2+} with high selectivity and affinity against other metal ions. a) The transfer curves (I_{sd}–V_g) were measured with various $C_{Zn^{2+}}$. b) A linear plot of the normalized calibrated response of $\Delta V_{g,Zn^{2+}}^{cal}/\Delta V_{g,Zn^{2+}}^{cal,max}$ as a function of $C_{Zn^{2+}}$. The $\Delta V_{g,Zn^{2+}}^{cal,max}$ represents the maximal electrical response of the FZ-3/SiNW-FET obtained at $C_{Zn^{2+}} = 8 \times 10^{-6}$ M. The inset shows a plot of $C_{Zn^{2+}}/\Delta V_{g,Zn^{2+}}^{cal}$ against $C_{Zn^{2+}}$ to determine the dissociation constant ($K_d = 12.0 \pm 3.2 \times 10^{-9}$ M) of the Zn^{2+}-FZ-3 complex by a least-squares fit to the Langmuir adsorption isotherm model. c) A semilogarithmic plot of the normalized calibrated responses of an FZ-3/SiNW-FET (red dots, with the data adopted from (a)) and a PTMS/SiNW-FET (black dots) in response to various $C_{Zn^{2+}}$ (100×10^{-15} to 8×10^{-6} M). The inset shows a set of the measured I_{sd}–V_g curves of a PTMS/SiNW-FET as a function of $C_{Zn^{2+}}$ (100×10^{-15} to 8×10^{-6} M). d) The target selectivity of an FZ-3/SiNW-FET. The FZ-3/SiNW-FET device was perfused with various metal ions ($M^{2+} = Zn^{2+}$, Fe^{2+}, Ca^{2+}, Mn^{2+}, or Mg^{2+}) at different concentrations. The data points presented in (b)–(d) are the mean ± SD with an average from three independent experiments ($n = 3$).

4 $NaHCO_3$, 5.6 glucose, pH 7.4) as the bath buffer in the following experiments and stimulated the neurons with AMPA. **Figure 3**a illustrates that AMPA activates a class of ionotropic glutamate receptors, that is, AMPARs, and depolarizes the membrane potential resulting in the fusion of synaptic vesicles with the plasma membrane. The neurotransmitter and Zn^{2+} are then coreleased at axon terminals.[43] Since AMPARs undergo rapid desensitization in the continuous presence of AMPA, the response will reach a plateau and then decline gradually.[44] Therefore, this treatment can represent the overexcitement of the neurons under physiological or pathological conditions.

To investigate the $C_{Zn^{2+}}^{ex}$ surrounding the AMPA-stimulated neurons, we calibrated the FZ-3/SiNW-FET, prior to cell experiments, by plotting the $\Delta V_{g,Zn^{2+}}^{cal}$ against various $C_{Zn^{2+}}$ measured in BSS buffer (Figure 3b). Despite the BSS buffer containing 1.26×10^{-3} M Ca^{2+} and 0.9×10^{-3} M Mg^{2+}, the K_d value ($12.1 \pm 3.9 \times 10^{-9}$ M) of Zn^{2+} with an FZ-3/SiNW-FET is similar to that obtained in the 50×10^{-3} M HEPES buffer (Figure 2b, $12.0 \pm 3.2 \times 10^{-9}$ M). This suggests that the interference from Ca^{2+} or Mg^{2+} to the binding between Zn^{2+} and FZ-3/SiNW-FET should be negligible. In the absence of neurons, AMPA (10×10^{-6} M) did not cause a conductance change in the FZ-3/SiNW-FET (Figure S6a, Supporting

Information); in contrast, in the presence of cultured neurons, the introduction of AMPA decreased the conductance, and the decrease was proportional to the C_{AMPA} applied (Figure 3c). The transfer curve (I_{sd}–V_g) measurements also showed that with the higher C_{AMPA} stimulation of neurons, a larger conductance change in the FZ-3/SiNW-FET and thus an increase in the released $C_{Zn^{2+}}^{ex}$ (Figure 3d). To calculate the $C_{Zn^{2+}}^{ex}$ surrounding the stimulated neurons (Figure 3e), we converted the ΔI_{sd} first to $\Delta V_{g,Zn^{2+}}^{cal}$ (from Figure 3d, as transformed earlier in Figure 2a,b, and Figure S4, Supporting Information) and then to $C_{Zn^{2+}}^{ex}$ (via the calibration curve of Figure 3b). Shown in Figure 3e are the resulting $\Delta V_{g,Zn^{2+}}^{cal} - C_{AMPA}$ and $C_{Zn^{2+}}^{ex} - C_{AMPA}$ relationships after the data conversions, where the higher C_{AMPA} applied, the larger $\Delta V_{g,Zn^{2+}}^{cal}$ change, and thus the higher $C_{Zn^{2+}}^{ex}$ released. Moreover, in Figure 3e, the $C_{Zn^{2+}}^{ex}$ increases from a basal level of $<0.6 \times 10^{-9}$ M (with the AMPA stimulant at $C_{AMPA} < 1 \times 10^{-6}$ M) to a plateau of $\approx 110 \times 10^{-9}$ M (at $C_{AMPA} > 13 \times 10^{-6}$ M). The 50% effective concentration (EC_{50}) of AMPA for elevating $C_{Zn^{2+}}^{ex}$ is $10.6 \pm 2.9 \times 10^{-6}$ M, which is similar to the reported $EC_{50} = 17 \times 10^{-6}$ M by detecting the AMPAR current with electrophysiology measurements[45] and close to our previous result of $EC_{50} = 10.3 \times 10^{-6}$ M by detecting the AMPA-induced K^+ release from neurons.[38]
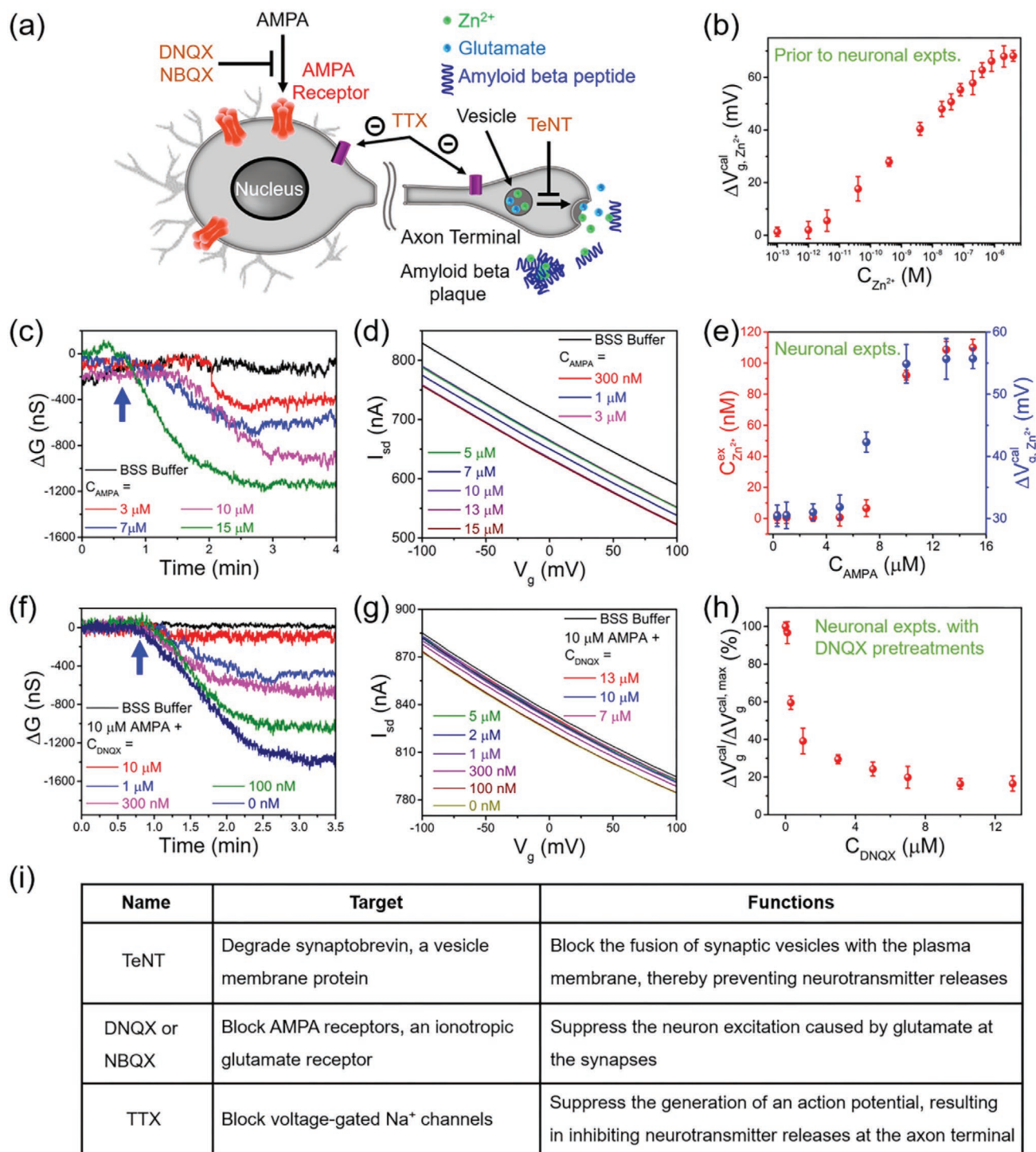
Figure 3. Detection of the Zn^{2+} released from excited neurons by FZ-3/SiNW-FET. a) An illustration of the AMPA-induced neurotransmitter release. AMPA binds the neuronal AMPAR and activates neurons to release neurotransmitters at the axon terminals. b) A calibration curve of the electrical responses of an FZ-3/SiNW-FET against various $C_{Zn^{2+}}$ (10^{-13}–10^{-5} M) in BSS buffer. The K_d calculated was $12.1 \pm 3.9 \times 10^{-9}$ M. The representative c) real-time measurements and d) transfer curve (I_{sd}–V_g) recordings of the Zn^{2+} released from excited neurons were conducted by FZ-3/SiNW-FET. The cultured cortical neurons placed atop an FZ-3/SiNW-FET in BSS buffer were stimulated with different C_{AMPA} (300×10^{-9} M -15×10^{-6} M). The arrows in (c) and (f) indicate the application of AMPA. e) The $C_{Zn^{2+}}^{ex}$ in the milieu of AMPA-stimulated neurons. The measured $\Delta V_{g,Zn^{2+}}^{cal}$ was converted to $C_{Zn^{2+}}^{ex}$ according to the calibration curve shown in (b). f,g) The blocking on excited neurons by DNQX. f) The real-time conductance changes (ΔG) and g) transfer curve (I_{sd}–V_g) shifts of neuronal experiments were recorded by FZ-3/SiNW-FET, where the neurons were pretreated with DNQX (0–13 $\times 10^{-6}$ M) and then stimulated with AMPA (10×10^{-6} M). h) The dose-dependent inhibition of the Zn^{2+} release by DNQX. The normalized $\Delta V_{g,Zn^{2+}}^{cal}/\Delta V_{g,Zn^{2+}}^{cal,max}$ is plotted against C_{DNQX}. i) A tabulated summary of the functions of channel blockers and their respective targets. The data points presented in (b), (e), and (h) are the mean $\pm$ SD with an average from three independent experiments ($n = 3$).

To verify that AMPARs could mediate the AMPA-induced Zn^{2+} release from neurons, we pretreated the neurons with 6,7-dinitroquinoxaline-2,3-dione (DNQX), an AMPAR selective antagonist (Figure 3a,i). DNQX (10×10^{-6} M) had no effect on the conductance of FZ-3/SiNW-FET in the absence of neurons (Figure S6b, Supporting Information), but suppressed the Zn^{2+} release from AMPA-stimulated neurons in a dose-dependent manner ($C_{DNQX} = 0.1–13 \times 10^{-6}$ M) (Figure 3f,g). Like the data processing from Figure 3d,e, we obtained Figure 3h (from Figure 3g) to reveal that DNQX pretreatment significantly inhibited AMPA-excited neuronal Zn^{2+} release with a half maximal inhibitory concentration (IC_{50}) of $1.0 \pm 0.3 \times 10^{-6}$ M (details in Section S3, Supporting Information). This is similar to the IC_{50} of 0.5×10^{-6} M obtained by inhibiting the binding of AMPA to AMPAR.[46] Another AMPAR antagonist, 2,3-dihydroxy-6-nitro-7-sulfamoyl-benzo[f]quinoxaline-2,3-dione (Figure 3a,i), showed the same effect on blocking AMPA-induced Zn^{2+} release with an IC_{50} of $186 \pm 23 \times 10^{-9}$ M (Figure S7, Supporting Information), similar to the IC_{50} reported previously (150×10^{-9} M).[47] These experiments demonstrate that the activation of AMPAR is able to induce Zn^{2+} release with the $C_{Zn^{2+}}^{ex}$ reaching $\approx 110 \times 10^{-9}$ M (Figure 3e). Nevertheless, because space existed between the neuron-seeded coverslip and the FZ-3/SiNW-FET, the $C_{Zn^{2+}}^{ex}$ may be underestimated. Consequently, the actual $C_{Zn^{2+}}^{ex}$ on the cell surface or at the synaptic clefts of the stimulated neurons is likely higher than 110×10^{-9} M.

To confirm that the AMPA-induced Zn^{2+} release is from the synaptic vesicles, we pretreated neurons with tetanus neurotoxin (TeNT, 50×10^{-9} M) for 1 h before AMPA stimulation. TeNT blocks the fusion of synaptic vesicles with the plasma membrane through the selective proteolysis of synaptobrevin, an integral membrane protein of synaptic vesicles (Figure 3a,i).[48] To verify the effectiveness of TeNT in blocking neurotransmission, we loaded neurons with the Ca^{2+}-sensitive dye Fluo-2 and locally stimulated a single neuron (Target) with AMPA (10×10^{-6} M) released from a micropipette with an opening of 1×10^{-6} M for 1 s. The inset of **Figure 4**a shows a representative fluorescence image of a Target and two postsynaptic neurons (Neighbor). The normalized fluorescence intensity (F/F_0) at the soma of each neuron was determined by comparing it (F) to the average fluorescence obtained before AMPA stimulation (F_0). The traces in Figure 4a show that brief AMPA stimulation transiently elevated the F/F_0 in the Target and Neighbor neurons. As summarized in Figure 4b, the average peak responses of the control group induced by AMPA were 2.4 ± 0.2 and 1.9 ± 0.1 for the Target and Neighbor neurons, respectively. To block neurotransmission, we pretreated the neurons with TeNT (50×10^{-9} M), DNQX (10×10^{-6} M), or tetrodotoxin (TTX) (1×10^{-9} M) before AMPA stimulation (Figure 4b). TTX blocks the voltage-gated Na^+ channels and terminates the initiation of an action potential (Figure 3a,i).[49,50] TeNT had no effect on the Target neurons (2.5 ± 0.4), but significantly suppressed the response of the Neighbor neurons (1.5 ± 0.1). These results suggest that TeNT has no effect on the neuron receiving AMPA stimulation but blocks neurotransmitter release at the axon terminal, suppressing the intracellular Ca^{2+} concentration (denoted by $[Ca^{2+}]_i$) in the postsynaptic neurons. In contrast, DNQX and TTX reduced the peak responses of both Target and Neighbor neurons; 1.3 ± 0.1 and

1.3 ± 0.1 for the DNQX group and 1.5 ± 0.1 and 1.3 ± 0.1 for the TTX group, respectively. These results reveal that both DNQX and TTX prevent Target neurons from activation thus diminishing neurotransmission.

To further confirm that TeNT blocked neurotransmission, we recorded the excitatory postsynaptic potential current (EPSC) from a whole-cell patched neuron under voltage-clamp mode with a holding potential of –70 mV and locally stimulated a presynaptic neuron with AMPA (10×10^{-6} M) (Figure 4c). The representative EPSC traces show that TeNT pretreatment reduced the AMPA-evoked EPSC. The average EPSC for the control group (without TeNT pretreatment) was 235.9 ± 36.9 pA, while TeNT (50×10^{-9} M) pretreatment significantly reduced the EPSC to 30.5 ± 5.2 pA. Accordingly, these results confirm that TeNT had no effect on the AMPA-evoked neuronal depolarization but greatly suppressed synaptic transmission by blocking neurotransmitter release.

To characterize the effect of TeNT on the $C_{Zn^{2+}}^{ex}$, we used the FZ-3/SiNW-FET to detect the Zn^{2+} released from neurons with or without a TeNT pretreatment (Figure 4d). AMPA stimulation resulted in an apparent drop in conductance for the control group; in contrast, TeNT pretreatment led to a small change in the conductance. In the inset of Figure 4d, the average change in the conductance was 9.3 ± 0.7 µS for the control group and was significantly suppressed to 1.0 ± 0.4 µS by TeNT pretreatment. This outcome demonstrates that synaptic vesicles are the main source responsible for the AMPA-induced elevation in $C_{Zn^{2+}}^{ex}$.

Zn^{2+} is involved in modulating the development of the nervous system and supporting versatile brain functions; however, excess Zn^{2+} causes degeneration of the nervous system.[51] $A\beta$ has two Zn^{2+}-binding sites with differential affinities ($K_d = 107 \times 10^{-9}$ and 5.2×10^{-6} M), and the high affinity site is rather important for the $A\beta$ aggregation.[52] Since the exact $C_{Zn^{2+}}^{ex}$ is controversial and our results show that the $C_{Zn^{2+}}^{ex}$ was measured $\approx 110 \times 10^{-9}$ M, it is not clear whether the Zn^{2+} released from neurons can trigger the formation of fibrillary $A\beta$. To this end, we designed an experiment by anchoring $A\beta$ peptides (1–40) on a SiNW-FET ($A\beta$/SiNW-FET) and monitoring a conductance change if Zn^{2+} binds to $A\beta$. Before the cell experiments, the response of the $A\beta$/SiNW-FET as a function of $C_{Zn^{2+}}$ was calibrated. **Figure 5**a shows the normalized $\Delta V_{g,Zn^{2+}}^{cal}/\Delta V_{g,Zn^{2+}}^{cal,max}$ of the $A\beta$/SiNW-FET increased as $C_{Zn^{2+}}$ rose and reached saturation at $C_{Zn^{2+}} > 10 \times 10^{-6}$ M. In the inset of Figure 5a, the K_d for the Zn^{2+}-$A\beta$ complex was $633 \pm 87 \times 10^{-9}$ M by fitting the data points with the Langmuir adsorption isotherm model. The interaction between Zn^{2+} and $A\beta$ was specific because even the highly concentrated Ca^{2+} or Mg^{2+} at 2×10^{-3} M caused little changes in the conductance of $A\beta$/SiNW-FET (Figure 5b).

To further verify that the Zn^{2+} released from neurons interacts with $A\beta$, we placed neurons atop an $A\beta$/SiNW-FET and stimulated the neurons with AMPA (10×10^{-6} M). The representative conductance traces in Figure 5c show that the AMPA stimulation resulted in a decrease in the conductance of $A\beta$/SiNW-FET with $\Delta G = 1.6 \pm 0.2$ µs (or $\Delta I_{sd} = 15.6 \pm 2.3$ nA, see Figure S8a, Supporting Information) corresponding to $C_{Zn^{2+}}^{ex} \approx 100 \times 10^{-9}$ M by the conversion process described in Figure S8 (Supporting Information). It is noteworthy that under an AMPA stimulation, the cultured cortical neurons released $C_{Zn^{2+}}^{ex} \approx 100 \times 10^{-9}$ M, which was determined consistently with
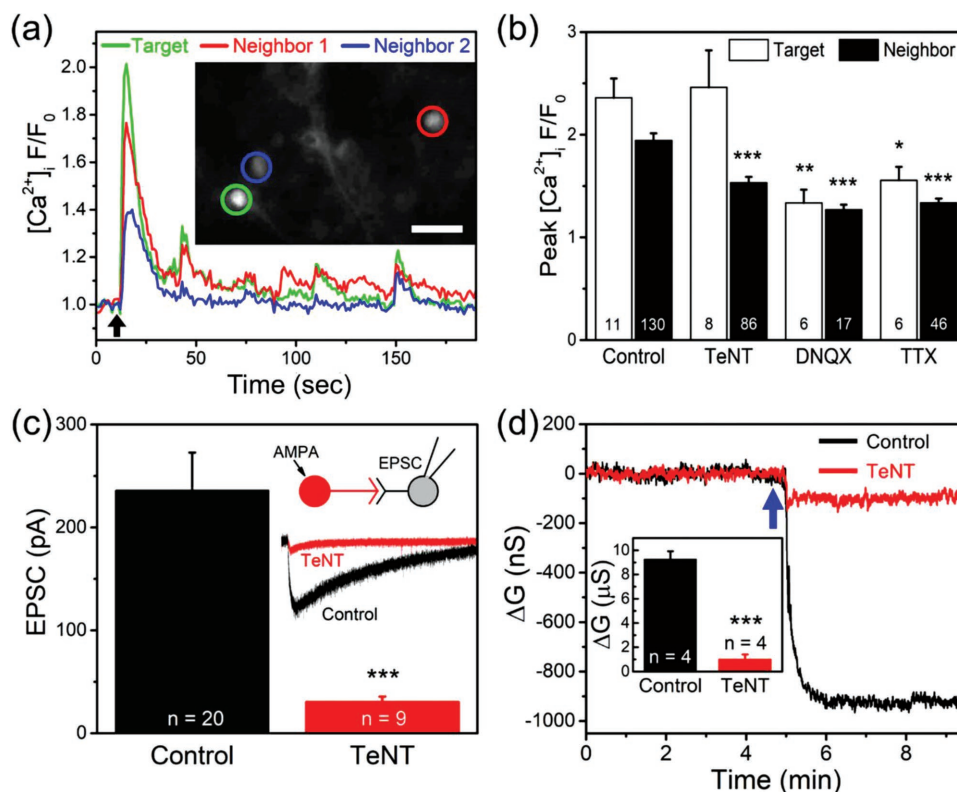
Figure 4. Blocking the neurotransmitter release with TeNT, DNQX, or TTX. a) Representative real-time $[Ca^{2+}]_i$ responses in neurons. Neurons were loaded with the Ca^{2+}-sensitive fluorescent dye, Fluo-2, and a single neuron was locally stimulated by AMPA (10×10^{-6} M) released from a micropipette for 1 s as indicated by the arrow. The fluorescence intensities in this stimulated neuron (Target) and the nearby postsynaptic neurons (Neighbor) were recorded. The fluorescence intensities were normalized to the average value prior to the AMPA stimulation (F/F_0). The inset shows the fluorescence image of the neurons of interest, where the circles indicated the regions of a Target neuron (green) and two Neighbor neurons (blue and red). Scale bar: 10 μm. b) Average AMPA-induced peak $[Ca^{2+}]_i$. Neurons were pretreated with TeNT (50×10^{-9} M), DNQX (10×10^{-6} M), and TTX (1×10^{-9} M) before the AMPA stimulation. The peak values of F/F_0 in the Target and Neighbor neurons were averaged. The number at the bottom of each column indicates how many independent measurements were conducted for this experiment. The presented data are the mean ± SD and were analyzed with the Student's t-test (*, **, and ***: $p < 0.05$, 0.01, and 0.001, respectively, when compared to the control group). c) AMPA-induced excitatory postsynaptic current (EPSC). A neuron was whole-cell patched in voltage-clamp mode with a holding potential of −70 mV. The number at the bottom of each column (i.e., $n = 20$ or $n = 9$) indicates the times of independent measurements conducted. The inset shows the EPSC traces recorded from the neurons without (as a control) or with a TeNT pretreatment, where a presynaptic neuron was stimulated with AMPA (10×10^{-6} M) from a micropipette. d) Real-time measurements of the conductance change (ΔG) of an FZ-3/SiNW-FET. The neurons without (as a control) or with a TeNT pretreatment were placed atop an FZ-3/SiNW-FET and stimulated with AMPA (marked by an arrow). The conductance was monitored in real time and the inset shows the average changes in conductance.

the FZ-3/SiNW-FET (Figure 3e) and Aβ/SiNW-FET (Figure S8c, Supporting Information) measurements. These measurements of Figure 5c and Figure S8 (Supporting Information) revealed that the $C_{Zn^{2+}}^{ex} \approx 100 \times 10^{-9}$ M was high enough to induce the Zn^{2+}-Aβ binding which may result in the formation of fibrillary Aβ.[53,54] In contrast, AMPA did not affect the conductance of Aβ/SiNW-FET in the absence of neurons (Figure 5c). Therefore, our results demonstrate that the Zn^{2+} released from synaptic vesicles can raise $C_{Zn^{2+}}^{ex}$ to ≈100 × 10^{-9} M, which is high enough to modulate various neuronal activities.

3. Conclusion

The formation of Aβ fibrillary aggregates is a pathogenic factor for Alzheimer's disease, but how the aggregation process initiates is not clear. Zn^{2+} can quickly bind Aβ (<1 ms),[52]

resulting in the formation of metastable oligomers that are toxic to neurons.[55] Although the Zn^{2+}-Aβ complex is the initial step in fibril formation,[54] most in vitro studies use high $C_{Zn^{2+}}^{ex}$ (>10 × 10^{-6} M, which is much higher than the $C_{Zn^{2+}}^{ex}$ in the brain), and it is not clear if the Zn^{2+}-Aβ complex forms in vivo. Our results demonstrate that the $C_{Zn^{2+}}^{ex}$ surrounding overexcited neurons can reach ≥100 × 10^{-9} M, which is enough for the binding of Zn^{2+} to the high affinity site of Aβ. Recently, Takeda et al. showed that treating the dentate granule cells in a rat hippocampal slice with 5×10^{-9} M of Aβ (1–42) in the presence of 10×10^{-9} M of Zn^{2+}, but not Cd^{2+}, Fe^{3+}, or Cu^{2+}, could attenuate the long-term potentiation.[56] Therefore, the Zn^{2+} coreleased with glutamate must be under strict regulation to avoid the formation of Aβ-Zn^{2+} complexes. In addition, this $C_{Zn^{2+}}^{ex}$ level is able to bind to NMDA receptors, which has a high affinity (≈nM level) against Zn^{2+}, to regulate neurotransmission.[6,16,17] In conclusion, our SiNW-FET system is a sensitive tool to
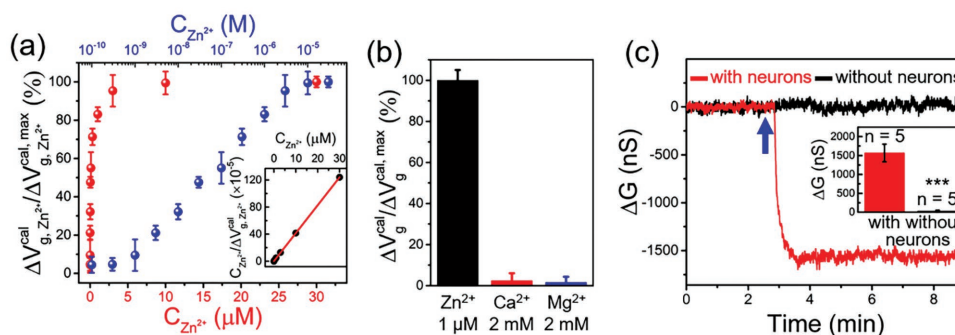
Figure 5. The responses of an Aβ/SiNW-FET to the Zn^{2+} released from AMPA-stimulated neurons. a) Normalized calibrated response. The $\Delta V_{g,Zn^{2+}}^{cal}/\Delta V_{g,Zn^{2+}}^{cal,max}$ of an Aβ/SiNW-FET was plotted as a function of $C_{Zn^{2+}}$ in a linear (red dots, bottom abscissa) or logarithmic (blue dots, top abscissa) scale. The $\Delta V_{g,Zn^{2+}}^{cal,max}$ represents the saturated $\Delta V_{g,Zn^{2+}}^{cal}$ measured at $C_{Zn^{2+}} = 50 \times 10^{-6}$ M. The inset shows a plot of $C_{Zn^{2+}}/\Delta V_{g,Zn^{2+}}^{cal}$ against $C_{Zn^{2+}}$, where $K_d = 633 \pm 87 \times 10^{-9}$ M for the Zn^{2+}-Aβ complex was determined. b) Target selectivity of an Aβ/SiNW-FET. The average responses of an Aβ/SiNW-FET to Zn^{2+} (1×10^{-6} M), Ca^{2+} (2×10^{-3} M), and Mg^{2+} (2×10^{-3} M) are presented. c) Real-time conductance change (ΔG) measured by Aβ/SiNW-FET. The ΔG of an Aβ/SiNW-FET, in contact with a coverslip seeded with (red trace) or without (black trace) neurons under an AMPA (10×10^{-6} M) stimulation (marked by an arrow), was monitored with the average ΔG presented in the inset. The data points presented in (a)–(c) are the mean ± SD with an average from three ($n = 3$ for (a) and (b)) and five ($n = 5$ for (c)) independent experiments, respectively, and were analyzed by the Student's t-test.

verify the $C_{Zn^{2+}}^{ex}$ in real time and examine how Zn^{2+} homeostasis modulates neuronal activities.

4. Experimental Section

Fabrication of SiNW-FET Devices: The SiNW-FET devices were fabricated with the procedures described previously.[37,57] Briefly, single-crystalline boron-doped SiNWs (B:Si = 1:4000) were grown catalytically in chemical vapor deposition reaction (460 °C for 12.5 min in 10 sccm Ar, 6 sccm SiH₄ (10% in He), and 15 sccm B₂H₆ (100 ppm in He) at a total chamber pressure of 25 Torr) through the vapor-liquid-solid growth mechanism with the assistance of 20 nm gold nanoparticles. The diameters of the as-synthesized p-type SiNWs were 20–30 nm. The SiNWs were transferred onto a photoresist (S1805)-patterned Si wafer with a 400 nm thick oxide layer using a contact printing method. The SiNW-FET devices were fabricated following standard photolithographic procedures, of which the details are described in Section S5 (Supporting Information) and can be found in ref. [38].

Immobilization of FluoZin-3 on an SiNW-FET: An SiNW-FET chip was rinsed thoroughly with ethanol and blown dry with N₂ gas. For the modification of CPTMS on the SiNW-FET, the FET chip was immersed in a 1% (v/v) ethanol solution containing CPTMS and incubated for 1 h to facilitate the reaction of the silane group of CPTMS with the silanol group on the SiNW surface to form a CPTMS/SiNW-FET (Figure S2, Supporting Information). This FET chip was rewashed with ethanol, blown dry with N₂, and cured at 110 °C for 5 min. An SiNW-FET was also modified with PTMS to form a PTMS/SiNW-FET with the identical procedures described above. The usage of a PTMS/SiNW-FET served as a control test, because the PTMS has a terminal methyl group and was unable to immobilize FZ-3 for detecting Zn^{2+} in the subsequent experiments.

The modification of FZ-3 on the CPTMS/SiNW-FET (Figure 1d) follows the procedures of acidification, esterification, and modification of FZ-3 on SiNWs (Figure S2, Supporting Information) with the details described in Section S4 (Supporting Information). The aim of this modification strategy is to preserve the chelator moiety in the original structure of FZ-3 during the immobilization process.

Electrical Measurement: Electrical measurements were performed with a protocol reported previously.[38] In brief, a lock-in amplifier (Stanford Research System, SR830) operated at $V_{sd} = 10$ mV, a modulation frequency of 79 Hz, and a time constant of 100 ms to monitor the conductance response of an FZ-3/SiNW-FET device was used. The

sample solution was either added directly onto the FZ-3/SiNW-FET chip surrounded by a PDMS wall (Figure 1a) or delivered through a PDMS microfluidic channel (L 6.26 mm × W 500 μm × H 50 μm) which was designed to couple with the FZ-3/SiNW-FET chip. An Ag/AgCl electrode, immersed in the sample solution throughout sensing experiments, was used as a solution gate with the voltage supplied by a data acquisition system (National Instruments, DAQ-NI2110) or was maintained at ground potential to minimize the electrical noise in real-time measurements. After each sensing experiment, the Zn^{2+} ions captured by FZ-3/SiNW-FET were washed off by flushing HEPES buffer containing 50×10^{-6} M of N,N,N′,N′-tetrakis(2-pyridylmethyl)ethylenediamine (TPEN, a Zn^{2+} chelator) through the PDMS microfluidic channel to return the FZ-3/SiNW-FET device to its original state without remaining the captured Zn^{2+} ions on the sensor surface.

Primary Culture of Cortical Neurons: The E14.5 embryos were isolated from a pregnant Sprague Dawley rat with a protocol described previously.[58] The procedure was complied with the Animal Welfare Regulations and approved by the Institutional Animal Care and Use Committee (Permit No. 103-30), National Taiwan University. In practice, the dissected embryo cortex was digested with papain and recovered in a cold Ca^{2+} and Mg^{2+}-free Hank's balanced salt solution (Ca^{2+}/Mg^{2+}-free HBSS, containing 5.33×10^{-3} M KCl, 0.44×10^{-3} M KH₂PO₄, 0.5×10^{-3} M, 138×10^{-3} M NaCl, 4×10^{-3} M NaHCO₃, 0.3×10^{-3} M Na₂HPO₄, and 5.6×10^{-3} M glucose, pH 7.4). The isolated cortical neurons were plated on 24 mm coverslips coated with poly-L-lysine at a density of 3×10^6 cell mL⁻¹ in neurobasal medium supplemented with B27.

Ca^{2+} Imaging and Electrophysiology: The changes of intracellular Ca^{2+} (represented by $[Ca^{2+}]_i$) were monitored with a protocol described before with some modifications.[58] In brief, the isolated cortical neurons cultured at days in vitro 9–12 were loaded with Fluo-2 acetoxymethyl ester (0.5×10^{-6} M) in HBSS for 20 min at room temperature. After washing, the neurons were incubated in HBSS and a single neuron was stimulated with AMPA (30×10^{-6} M) released from a micropipette with a tip opening of 1 μm positioned at 30 μm from the Target neuron. The images were captured every second for fluorescence intensity analysis in the stimulated Target and Neighbor neurons. The values of the fluorescence intensity (F) were normalized to the average intensity before stimulation (F_0) and the $[Ca^{2+}]_i$ were represented by F/F_0.

For excitatory postsynaptic current recording, the neurons were patched in whole-cell mode under voltage-clamp with a holding potential of −70 mV as described before.[59] The pipette solution consisted of 120×10^{-3} M aspartic acid, 5×10^{-3} M MgCl₂, 40×10^{-3} M HEPES, 0.1×10^{-3} M EGTA, 2×10^{-3} M ATP, and 0.3×10^{-3} M GTP, pH 7.3 with CsOH (310×10^{-3} M mOsm kg⁻¹) and the bath buffer was HBSS. To

record the whole-cell postsynaptic current, a nearby presynaptic neuron was stimulated with AMPA (10×10^{-6} M) released from a micropipette for 1 s. The amplifier for the recording was EPC10 and controlled by Pulse software (HEKA).

Statistical Analysis: The data presented are the mean ± standard deviation (SD); the significance was analyzed using a Student's *t*-test. The sample numbers for each experiment are presented in the corresponding figures. Differences are considered statistically significant when $p < 0.05$.

Supporting Information

Supporting Information is available from the Wiley Online Library or from the author.

Acknowledgements

Conflict of Interest

The authors declare no conflict of interest.

Keywords

[1] A. Q. Truong-Tran, J. Carter, R. E. Ruffin, P. D. Zalewski, *Biometals* **2001**, *14*, 315.

[2] F. Y.-H. Wu, C. W. Wu, *Annu. Rev. Nutr.* **1987**, *7*, 251.

[3] W. Maret, C. Jacob, B. L. Vallee, E. H. Fischer, *Proc. Natl. Acad. Sci. USA* **1999**, *96*, 1936.

[4] K. A. Jackson, R. A. Valentine, L. J. Coneyworth, J. C. Mathers, D. Ford, *Biochem. Soc. Trans.* **2008**, *36*, 1262.

[5] P. Bonaventura, G. Benedetti, F. Albarède, P. Miossec, *Autoimmun. Rev.* **2015**, *14*, 277.

[6] T. G. Smart, X. Xie, B. J. Krishek, *Prog. Neurobiol.* **1994**, *42*, 393.

[7] R. A. Colvin, C. P. Fontaine, M. Laskowski, D. Thomas, *Eur. J. Pharmacol.* **2003**, *479*, 171.

[8] A. T. Miles, G. M. Hawksworth, J. H. Beattie, V. Rodilla, *Crit. Rev. Biochem. Mol. Biol.* **2000**, *35*, 35.

[9] M. Aschner, M. G. Cherian, C. D. Klaassen, R. D. Palmiter, J. C. Erickson, A. I. Bush, *Toxicol. Appl. Pharmacol.* **1997**, *142*, 229.

[10] D. T. Dexter, F. R. Wells, A. J. Lee, F. Agid, Y. Agid, P. Jenner, C. D. Marsden, *J. Neurochem.* **1989**, *52*, 1830.

[11] A. P. Smith, N. M. Lee, *Amyotrophic Lateral Scler.* **2007**, *8*, 131.

[12] A. Deshpande, H. Kawai, R. Metherate, C. G. Glabe, J. Busciglio, *J. Neurosci.* **2009**, *29*, 4004.

[13] K.-L. Lim, C.-W. Zhang, *Front. Neurol.* **2013**, *4*, 33.

[14] C. J. Frederickson, *Int. Rev. Neurobiol.* **1989**, *31*, 145.

[15] K. Vogt, J. Mellor, G. Tong, R. Nicoll, *Neuroendocrinology* **2000**, *26*, 187.

[16] Y. Z. Huang, E. Pan, Z.-Q. Xiong, J. O. McNamara, *Neuroendocrinology* **2008**, *57*, 546.

[17] A. S. Nakashima, R. H. Dyck, *Brain Res. Rev.* **2009**, *59*, 347.

[18] S. Y. Assaf, S.-H. Chung, *Nature* **1984**, *308*, 734.

[19] Y. Li, C. J. Hough, S. W. Suh, J. M. Sarvey, C. J. Frederickson, *J. Neurophysiol.* **2001**, *86*, 2597.

[20] J. Qian, J. L. Noebels, *J. Physiol.* **2005**, *566*, 747.

[21] R. B. Thompson, W. O. Whetsell Jr., B. P. Maliwal, C. A. Fierke, C. J. Frederickson, *J. Neurosci. Methods* **2000**, *96*, 35.

[22] C. J. Frederickson, L. J. Giblin, A. Krężel, D. J. McAdoo, R. N. Muelle, Y. Zeng, R. V. Balaji, R. Masalha, R. B. Thompson, C. A. Fierke, J. M. Sarvey, M. de Valdenebro, D. S. Prough, M. H. Zornow, *Exp. Neurol.* **2006**, *198*, 285.

[23] A. R. Kay, *J. Neurosci.* **2003**, *23*, 6847.

[24] S. L. Sensi, P. Paoletti, A. I. Bush, I. Sekler, *Nat. Rev. Neurosci.* **2009**, *10*, 780.

[25] K. He, E. Aizenman, *J. Neurochem.* **2010**, *114*, 452.

[26] A. I. Bush, W. H. Pettingell, G. Multhaup, M. D. Paradis, J. P. Vonsattel, J. F. Gusella, K. Beyreuther, C. L. Masters, R. E. Tanzi, *Science* **1994**, *265*, 1464.

[27] D. Mizuno, M. Kawahara, *Int. J. Mol. Sci.* **2013**, *14*, 22067.

[28] C. J. Frederickson, M. A. Klitenick, W. I. Manton, J. B. Kirkpatrick, *Brain Res.* **1983**, *273*, 335.

[29] M. Yokoyama, J. Koh, D. W. Choi, *Neurosci. Lett.* **1986**, *71*, 351.

[30] A. Takeda, H. Tamano, *Expert Opin. Ther. Targets* **2015**, *19*, 1051.

[31] Y. Cui, Q. Wei, H. Park, C. M. Lieber, *Science* **2001**, *293*, 1289.

[32] T.-S. Pui, A. Agarwal, F. Ye, Z.-Q. Tou, Y. Huang, P. Chen, *Nanoscale* **2009**, *1*, 159.

[33] K.-I. Chen, B.-R. Li, Y.-T. Chen, *Nano Today* **2011**, *6*, 131.

[34] Y. Wang, T. Wang, P. Da, M. Xu, H. Wu, G. Zheng, *Adv. Mater.* **2013**, *25*, 5177.

[35] Z. C. Lin, B. Cui, *Nat. Nanotechnol.* **2014**, *9*, 94.

[36] B.-R. Li, C.-C. Chen, U. R. Kumar, Y.-T. Chen, *Analyst* **2014**, *139*, 1589.

[37] B.-R. Li, Y.-J. Hsieh, Y.-X. Chen, Y.-T. Chung, C.-Y. Pan, Y.-T. Chen, *J. Am. Chem. Soc.* **2013**, *135*, 16034.

[38] A. Anand, C.-R. Liu, A.-C. Chou, W.-H. Hsu, R. K. Ulaganathan, Y.-C. Lin, C.-A. Dai, F.-G. Tseng, C.-Y. Pan, Y.-T. Chen, *ACS Sens.* **2017**, *2*, 69.

[39] K. R. Gee, Z.-L. Zhou, W.-J. Qian, R. Kennedy, *J. Am. Chem. Soc.* **2002**, *124*, 776.

[40] I. Marszałek, A. Krężel, W. Goch, I. Zhukov, I. Paczkowska, W. Bal, *J. Inorg. Biochem.* **2016**, *161*, 107.

[41] F. N. Ishikawa, M. Curreli, H.-K. Chang, P.-C. Chen, R. Zhang, R. J. Cote, M. E. Thompson, C. Zhou, *ACS Nano* **2009**, *3*, 3969.

[42] R. Y. Tsien, *Biochemistry* **1980**, *19*, 2396.

[43] U. Schenk, C. Verderio, F. Benfenati, M. Matteoli, *EMBO J.* **2003**, *22*, 558.

[44] K. B. Hansen, H. Yuan, S. F. Traynelis, *Curr. Opin. Neurobiol.* **2007**, *17*, 281.

[45] D. E. Jane, K. Hoo, R. Kamboj, M. Deverill, D. Bleakman, A. Mandelzys, *J. Med. Chem.* **1997**, *40*, 3645.

[46] T. Honore, S. N. Davies, J. Drejer, E. J. Fletcher, P. Jacobsen, D. Lodge, F. E. Nielsen, *Science* **1988**, *241*, 701.

[47] M. J. Sheardown, E. O. Nielsen, A. J. Hansen, P. Jacobsen, T. Honore, *Science* **1990**, *247*, 571.

[48] E. Link, L. Edelmann, J. H. Chou, T. Binz, S. Yamasaki, U. Eisel, M. Baumert, T. C. Südhof, H. Niemann, R. Jahn, *Biochem. Biophys. Res. Commun.* **1992**, *189*, 1017.

[49] R. Chen, S.-H. Chung, *Biochem. Biophys. Res. Commun.* **2014**, *446*, 370.

[50] M. Ikeda, M. Ikeda, *J. Neurosci.* **2014**, *34*, 12029.

[51] S. D. Gower-Winter, C. W. Levenson, *Biofactors* **2012**, *38*, 186.

[52] J. Guo, L. Yu, Y. Sun, X. Dong, *J. Phys. Chem. B* **2017**, *121*, 3909.

ADVANCED
SCIENCE NEWS

www.advancedsciencenews.com

NANO · MICRO

small

www.small-journal.com

[53] Y. Miller, B. Ma, R. Nussinov, *Proc. Natl. Acad. Sci. USA* **2010**, *107*, 9490.

[54] L. Ye, J. Rasmussen, S. A. Kaeser, A.-M. Marzesco, U. Obermüller, J. Mahler, J. Schelle, J. Odenthal, C. Krüger, S. K. Fritschi, L. C. Walker, M. Staufenbiel, F. Baumann, M. Jucker, *EMBO Rep.* **2017**, *18*, 1536.

[55] I. Solomonov, E. Korkotian, B. Born, Y. Feldman, A. Bitler, F. Rahimi, H. Li, G. Bitan, I. Sagi, *J. Biol. Chem.* **2012**, *287*, 20555.

[56] A. Takeda, H. Tamano, M. Tempaku, M. Sasaki, C. Uematsu, S. Sato, H. Kanazawa, Z. L. Datki, P. A. Adlard, A. I. Bush, *J. Neurosci.* **2017**, *37*, 7253.

[57] F. Patolsky, G. Zheng, C. M. Lieber, *Nat. Protoc.* **2006**, *1*, 1711.

[58] M.-P. Wu, L.-S. Kao, H.-T. Liao, C.-Y. Pan, *Brain Res.* **2008**, *1201*, 41.

[59] M.-Y. Chou, C.-Y. Lee, H.-H. Liou, C.-Y. Pan, *Neuropharmacology* **2014**, *83*, 54.

1704439 (10 of 10)

NANO MICRO

small

Supporting Information

The Extracellular Zn^{2+} Concentration Surrounding Excited Neurons Is High Enough to Bind Amyloid-β Revealed by a Nanowire Transistor

Ankur Anand, Chih-Hung Chi, Subhasree Banerjee, Ming-Yi Chou, Fan-Gang Tseng, Chien-Yuan Pan,* and Yit-Tsong Chen*

S1. Materials and Reagents

FluoZin-3, Dulbecco's modified Eagle's medium, and other cell cultured medium (e.g., B27) were purchased from Invitrogen (Carlsbad, CA, USA). Fluo-2 acetoxymethyl ester was purchased from Teflabs (Austin, TX, USA). 3-chloropropyltrimethoxysilane (CPTMS), propyltrimethoxysilane (PTMS) HEPES (4-(2-hydroxyethyl)-1-piperazineethanesulfonic acid), α-amino-3-hydroxy-5-methyl-4-isoxazolepropionic (AMPA), 6,7-dinitroquinoxaline-2,3-dione (DNQX), 2,3-dihydroxy-6-nitro-7-sulfamoyl-benzo[f]quinoxaline-2,3-dione (NBQX), tetanus toxin (TeNT), methanol, and the other chemicals not indicated were purchased from Sigma-Aldrich. Deionized water (>18 MΩ·cm) obtained from a purification system (Millipore Synergy) was used throughout the experiments.

S2. Dissociation Constant

The dissociation constant (K_d) of the Zn^{2+}-FZ-3 complex was determined by a least-squares fit of the $C_{Zn^{2+}} / \Delta V_{g, Zn^{2+}}^{cal}$ vs. $C_{Zn^{2+}}$ data (in the inset of Figure 2b) to the Langmüir adsorption isotherm model:

$$\frac{C_{Zn^{2+}}}{\Delta V_{g, Zn^{2+}}^{cal}} = \frac{1}{\Delta V_{g, Zn^{2+}}^{cal, max}} \cdot C_{Zn^{2+}} + \frac{1}{\Delta V_{g, Zn^{2+}}^{cal, max}} \cdot K_d \qquad \text{(Equation S1)}$$

where the relative $\Delta V_{g, Zn^{2+}}^{cal}$ is defined as $\Delta V_{g, Zn^{2+}}^{cal} (\%) = (\Delta V_{g, Zn^{2+}}^{cal} - \Delta V_{g, 0}^{cal}) / \Delta V_{g, 0}^{cal} \times 100$ (%), $\Delta V_{g, 0}^{cal}$ is the calibrated response at $C_{Zn^{2+}} = 0$ M that induces no detectable signal, and $\Delta V_{g, Zn^{2+}}^{cal, max}$ is the saturated calibrated response at high $C_{Zn^{2+}}$. The same protocol was applied to calculate the K_d of the Zn^{2+}-Aβ complex (in the inset of Figure 5a).

S3. Estimation of IC$_{50}$ Values by means of a Boltzmann Sigmoidal Function

The IC$_{50}$ value was determined by fitting the dose response curve (Figure 3h and S7c) to a Boltzmann sigmoidal function with Origin 9.1 (OriginLab, MA, USA).

$$y = \frac{A_1 - A_2}{1 + e^{\frac{(x - x_0)}{dx}}} + A_2 \qquad \text{(Equation S2)}$$

where, A_1, and A_2 are the values of the lower and upper limits on the dose-response curve, respectively, x is the DNQX or NBQX concentration, x_0 is the dose corresponding to the midpoint (i.e., IC$_{50}$) between A_1 and A_2, and dx denotes the slope of the dose-response curve.

S4. Immobilization of FluoZin-3 on an SiNW-FET

The modification of 3-chloropropyltrimethoxysilane (CPTMS) on the SiNW-FET was described in Experimental Section of the main text. After the CPTMS-modification, the FET chip was washed with ethanol and next for the modification of FZ-3.

The modification of FZ-3 on the CPTMS/SiNW-FET was via the acidification and esterification procedures, followed by the covalent linking of FZ-3 on the SiNWs (Figure S2). The aim of this modification strategy is to preserve the chelator moiety in the original structure of FZ-3 during the immobilization process. In the modification, all items of glassware and plastics were immersed in 2 M HNO$_3$ overnight to prevent the contamination of Zn^{2+} leaching from the lab wares and subsequently were washed thoroughly with deionized water (18 MΩ). The entire procedures were carried out in the dark and under the inert (Ar) atmosphere. The solvents used were of anhydrous grade and deionized water (18 MΩ) was used throughout this study.

The vial containing aqueous solution of FZ-3 was acidified with 1 M hydrochloric acid (1 mL) with a mild stir for 10 min. The resulting bright orange-colored solution was extracted with ethyl acetate three times (3×2 mL), dried over anhydrous Na$_2$SO$_4$, and evaporated under

reduced pressure to yield a brown residue. The residue was dissolved in methanol (0.5 mL) and concentrated H_2SO_4 (10 % v/v solution in methanol) was added and stirred for 2 hours at 65 ℃. After the solution was cooled to room temperature, methanol was removed under reduced pressure and the excess H_2SO_4 was neutralized with saturated $NaHCO_3$. The resulting solution was extracted with dichloromethane three times (3×2 mL), dried over anhydrous Na_2SO_4, and evaporated under reduced pressure to yield a reddish brown residue (FZ-3a). This residue was further dissolved in acetone, resulting in the reappearance of an orange color, where the final ~1 µM of FZ-3a solution was obtained.

The modification of FZ-3 on CPTMS/SiNWs was carried out by adding 10 µL of the FZ-3 solution (1 µM in acetone) on a CPTMS/SiNW-FET chip. Sodium methoxide (prepared by dissolving 4g NaOH in 100 mL of methanol) was added to provide a mildly alkaline condition to facilitate the reaction. The chip was incubated for 1 hour under ambient atmosphere. Thereafter, the chip was washed with ethanol, blown dry with N_2 gas, and immersed in a methanol solution containing 0.1 M KOH at 25 °C for 2 hours.

A comparison of the modification of FZ-3 on a CPTMS-modified or a PTMS-modified SiO_2/Si substrate was carried out to confirm the successful immobilization of FZ-3 on the SiO_2/Si surface. As displayed in Figure S3a, a homogenous fluorescence image of the Zn^{2+}-bound FZ-3-modified SiO_2/Si substrate, obtained in a confocal microscope (Leica, TCS SP5), indicates the uniform modification of FZ-3 on the CPTMS-modified SiO_2/Si surface. In contrast, no fluorescence was observed on the PTMS-modified SiO_2/Si surface (Figure S3b). Furthermore, as shown in Figure S3c, the fluorescence spectrum of an FZ-3-modified SiO_2/Si substrate with λ_{max} ~ 516 nm is consistent with that of the FZ-3 dissolved in HEPES buffer obtained from a spectrofluorometer (Jasco, FP-6500), signifying the preserved Zn^{2+}-binding capability of the chromophoric moiety of FZ-3 after the chemical modification process. In addition, the absorption spectrum of FZ-3 (Figure S3c) in HEPES buffer at pH 7.4 was

obtained for reference. The modification of FZ-3 on an SiNW-FET was also examined by measuring the shifts of the transfer curves (I_{sd}–V_g). As depicted in Figure S3d, after the FZ-3 modification, the transfer curve of FZ-3/SiNW-FET (red) shifted upward, relative to that of CPTMS/SiNW-FET (black), indicating a gating effect of negatively charged FZ-3 on the *p*-type SiNW-FET. Comparatively, the exposure of the FZ-3/SiNW-FET to 1 µM of Zn^{2+} in HEPES buffer, the transfer curve (blue) shifted downward, which is consistent with the gating effect due to the positively charged Zn^{2+}.

S5. Fabrication of SiNW-FET Devices

The SiNW-FET devices were fabricated following standard photolithographic procedures. The metal contact regions (defined by photolithography) were cleaned with oxygen plasma (100 sccm and 30 W); meanwhile, the native silica sheath of the SiNW in the contact area was removed with a buffered oxide etching (BOE) solution. The metal contacts (70 nm Ni and 100 nm Al in thickness) with interdigitated patterns defined by a photomask were deposited by thermal evaporation. The separation between the source and drain electrodes is 3 µm. After lift-off, the SiNW-FET devices were further annealed in forming gas (10 % H_2 and 90 % N_2) at 360 °C for 3 min to ensure a good electrical contact between SiNWs and metal electrodes. The silica insulating layer on the SiNW surface could prevent the charge transfer between the SiNW-FET and analyte molecules as well as electrical leakage in the subsequent biosensing measurements in aqueous solution.
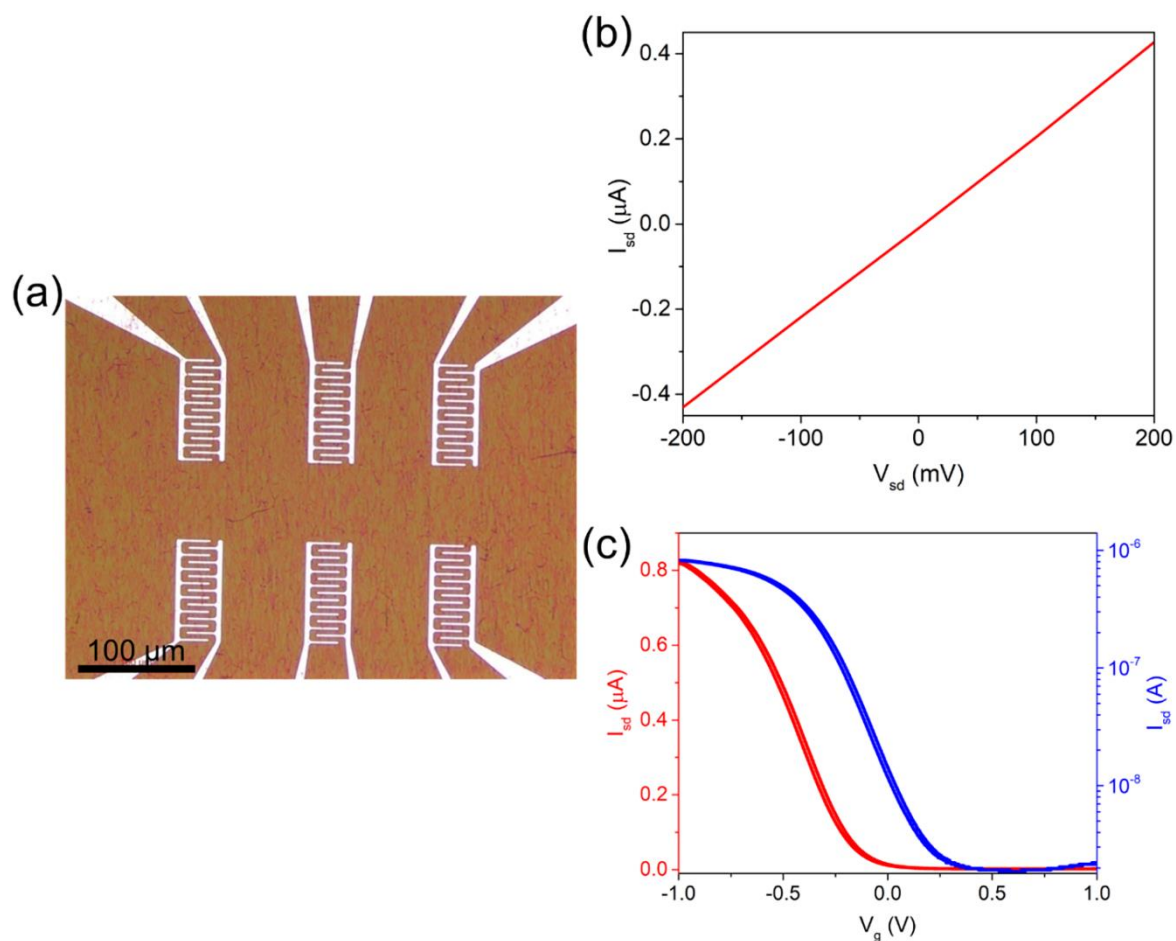
Figure S1. Device design and electrical characterizations of a representative SiNW-FET biosensor. (a) A chip contains six pairs of SiNW-FET devices. Each device comprises several tens of single-crystalline boron-doped SiNWs (~20 nm in diameter each) as conducting channels between the interdigitated source and drain electrodes. (b) A representative output curve (i.e., an I_{sd}–V_{sd} plot) of an SiNW-FET device was measured in an ambient condition. (c) The transfer curve (i.e., an I_{sd}–V_g plot) of a bare SiNW-FET immersed in HEPES buffer solution was measured at $V_{sd} = 10$ mV by a lock-in amplifier with a modulation frequency of 79 Hz and a time constant of 100 ms. The V_g was scanned with the voltage supplied from a data acquisition system (National Instruments, DAQ-NI2110) via an Ag/AgCl reference electrode. The I_{sd} is presented on a linear (red) or logarithmic (blue) scale.
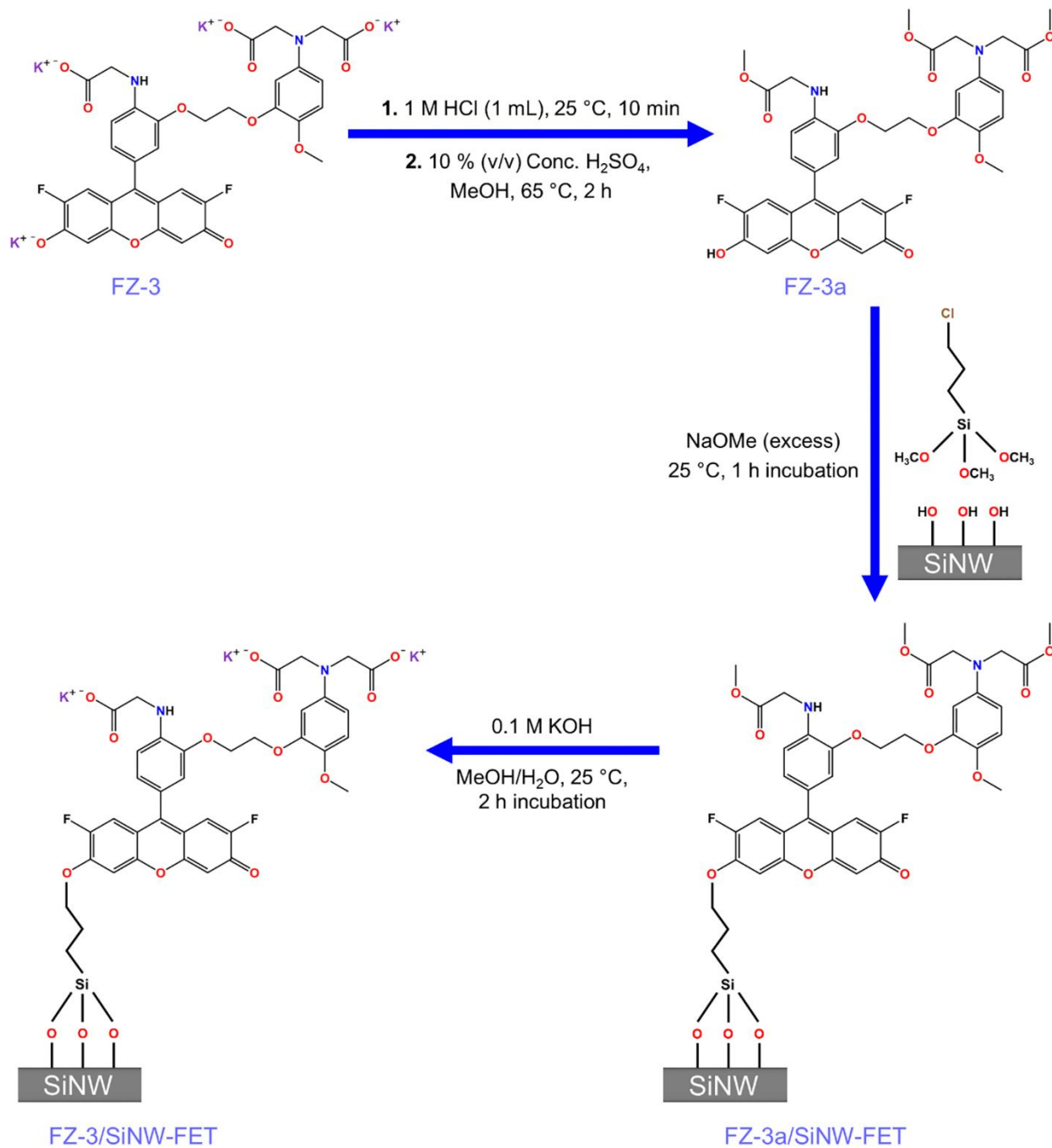
Figure S2. Covalently linking the FluoZin-3 (FZ-3) molecule to the surface of SiNW. The experimental procedures are described in Experimental Section of the main text and Section S4 of the Supporting Information.
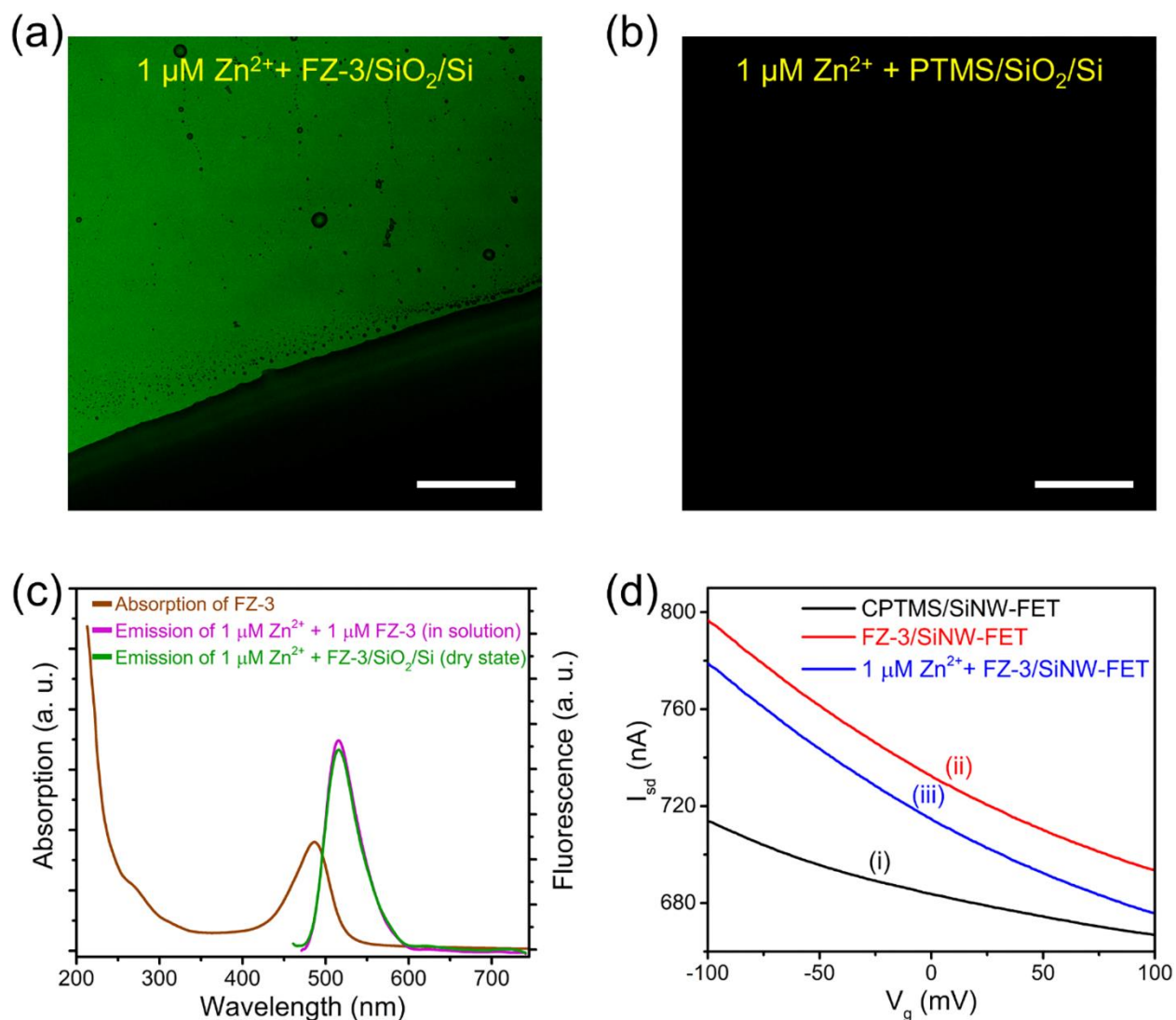
Figure S3. An FZ-3/SiNW-FET in response to Zn^{2+}. (a) A fluorescence image from a SiO_2/Si substrate modified with FZ-3 (in the upper part) in the presence of Zn^{2+} (1 μM). Scale bar: 100 μm. (b) A PTMS-modified SiO_2/Si substrate had no fluorescence signal in the presence of Zn^{2+} (1 μM). Scale bar: 100 μm. (c) The absorption (brown trace) and emission (green trace) spectra of the FZ-3 immobilized on a SiO_2/Si substrate. The emission spectrum of FZ-3 in HEPES buffer solution (purple trace) is also presented for reference. While these three spectra were obtained in the presence of 1 μM of Zn^{2+}, the concentrations of FZ-3 were different in the solution and dry-state measurements. (d) The transfer curves of an SiNW-FET device were measured in HEPES buffer solution during the modification processes of (i) immobilizing CPTMS (to become a CPTMS/SiNW-FET, black trace), (ii) anchoring FZ-3 (to

form an FZ-3/SiNW-FET, red trace), and (iii) introducing 1 µM of Zn^{2+} to the FZ-3/SiNW-FET (blue trace). The upward/downward shifts of the transfer curves are caused by a gating effect on the SiNW-FET device due to the charged species on the SiNW surface.
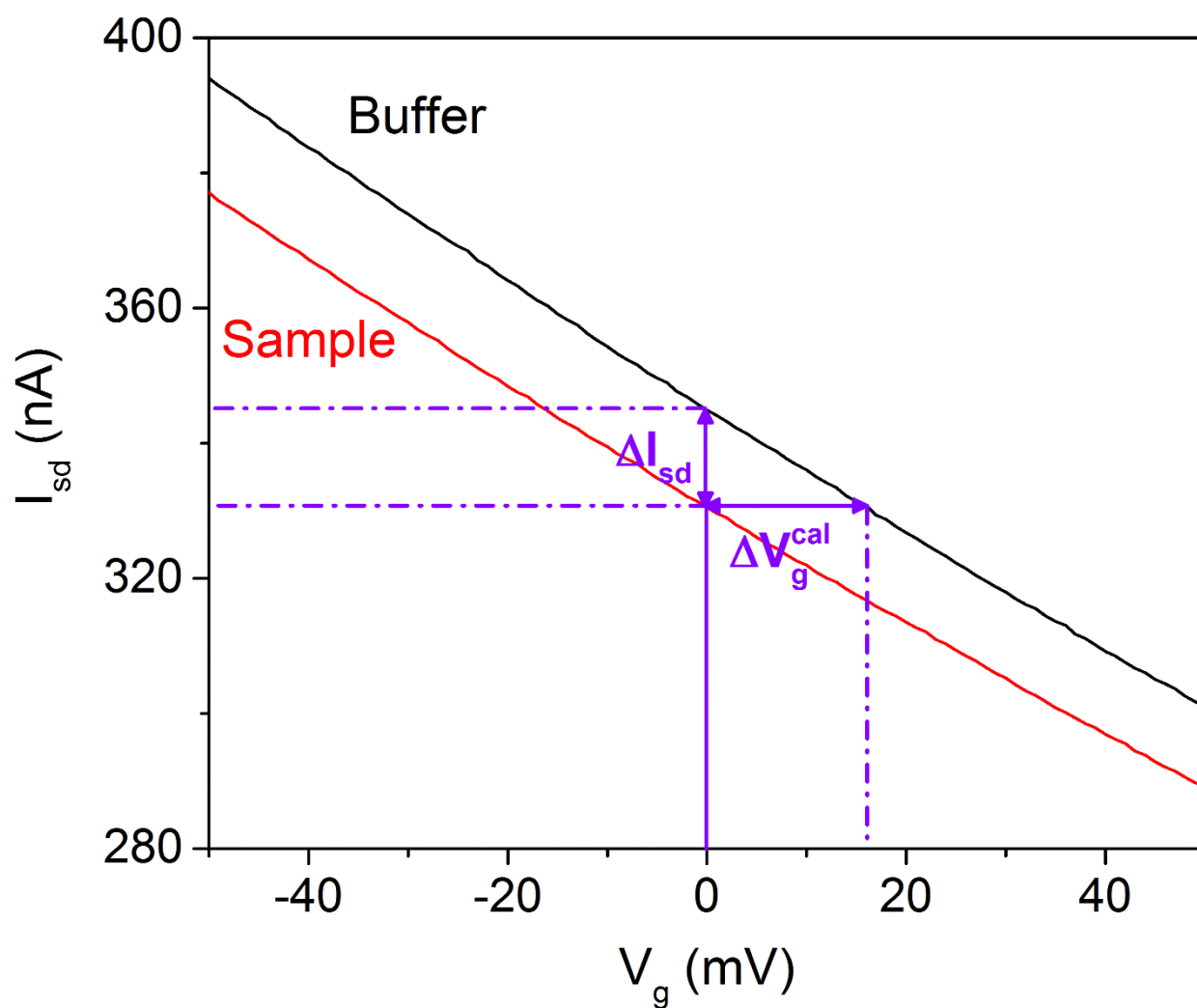
Figure S4. To avoid device-to-device variation in the detection sensitivity with different SiNW-FETs, the measured current change due to the receptor-target binding (ΔI_{sd} at $V_g = 0$ mV, relative to the buffer solution) was converted to the changes in V_g (termed the calibrated response and represented by ΔV_g^{cal}) according to the I_{sd}–V_g transfer curve of that SiNW-FET device.
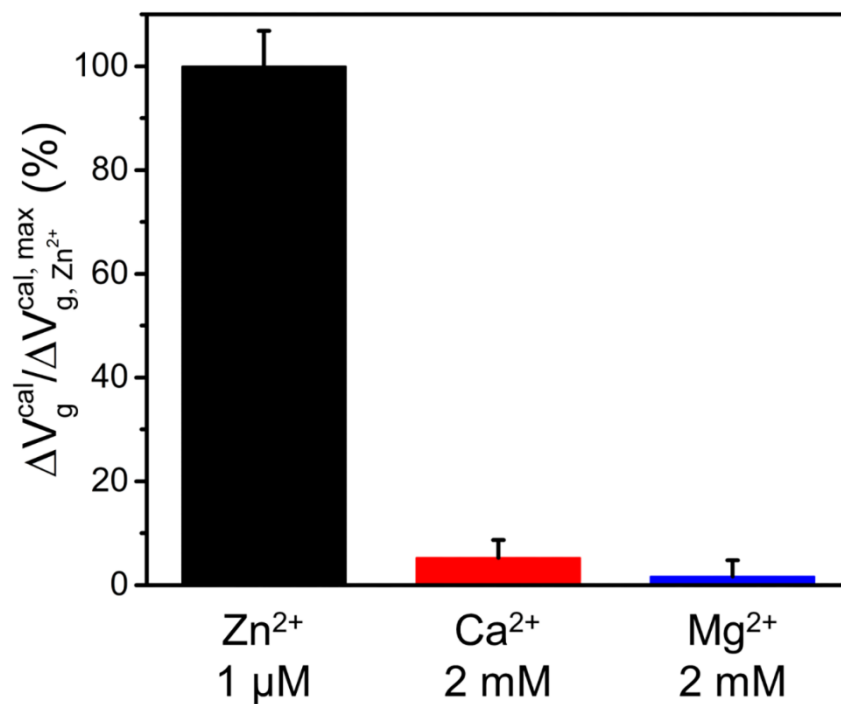
Figure S5. The detection selectivity of an FZ-3/SiNW-FET. The average responses of an FZ-3/SiNW-FET to Zn^{2+} (1 μM), Ca^{2+} (2 mM), and Mg^{2+} (2 mM) in 50 mM HEPES buffer are presented for comparison. The data points presented are the mean ± SD with an average from three independent experiments (n = 3).
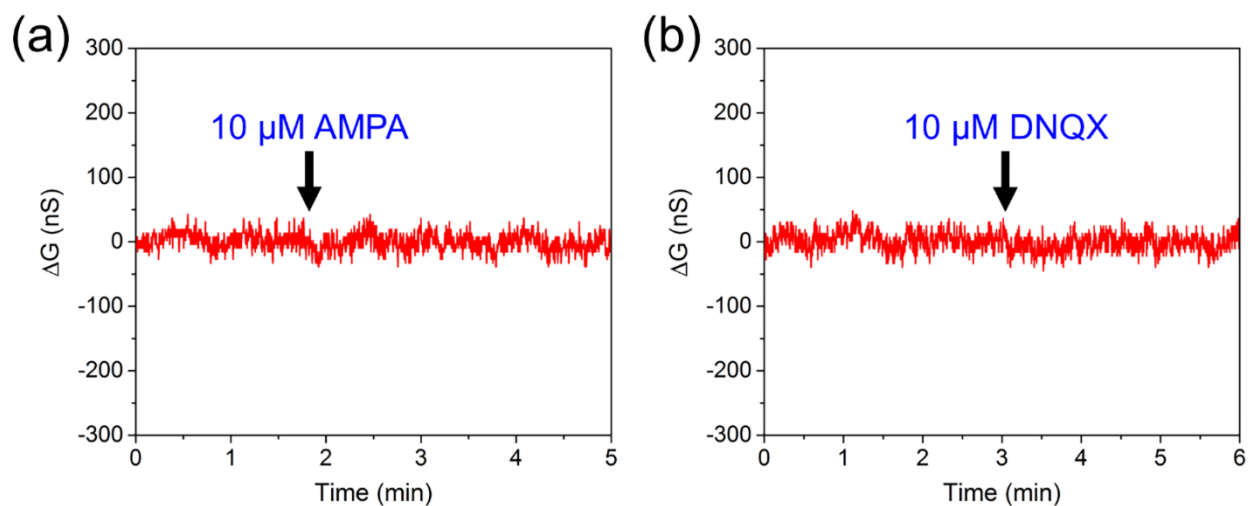
Figure S6. In the absence of cortical neurons, no conductance changes of an FZ-3/SiNW-FET were observed by adding (a) AMPA (10 μM) and (b) DNQX (10 μM) on the FZ-3/SiNW-FET device. The arrows indicate the sample applications.
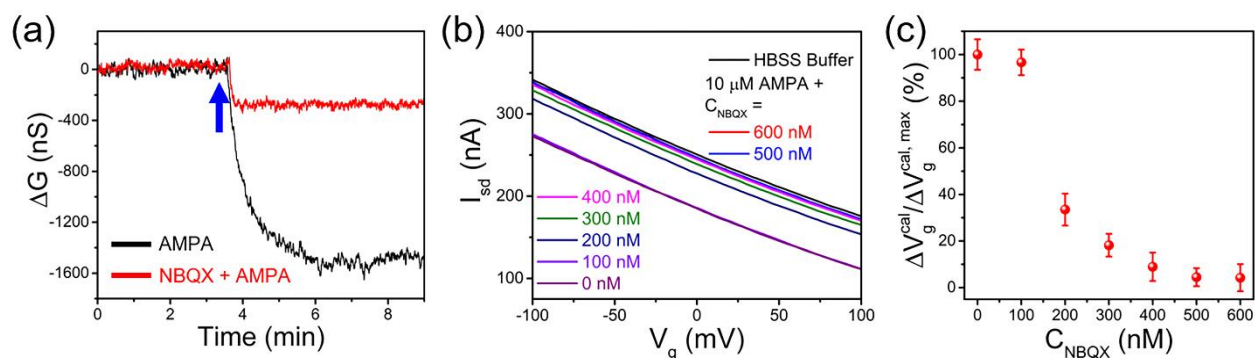
Figure S7. Suppression of the AMPA-induced Zn^{2+} release by NBQX. Neurons seeded on a coverslip were placed atop an FZ-3/SiNW-FET and were treated with NBQX (C_{NBQX} = 0–600 nM) before AMPA (10 μM) stimulation. (a) Representative conductance traces of an FZ-3/SiNW-FET. The conductance change (ΔG) of an FZ-3/SiNW-FET covered with neurons in the presence (red trace) or absence (black trace) of NBQX (200 nM) was recorded. The arrow indictes the application of AMPA (10 μM). Since the pretreatment of cortical neurons with 200 nM of NBQX could only partially block the AMPAR, a small amount of Zn^{2+} was still released from the neurons and detected by the FZ-3/SiNW-FET. (b) The corresponding measured I_{sd}–V_g curves with various C_{NBQX}. (c) The normalized $\Delta V_{g,Zn^{2+}}^{cal} / \Delta V_{g,Zn^{2+}}^{cal,max}$ was converted from the data in (b). The use of NBQX to block the AMPA-induced Zn^{2+} release with an IC_{50} of 186 ± 23 nM was determined.
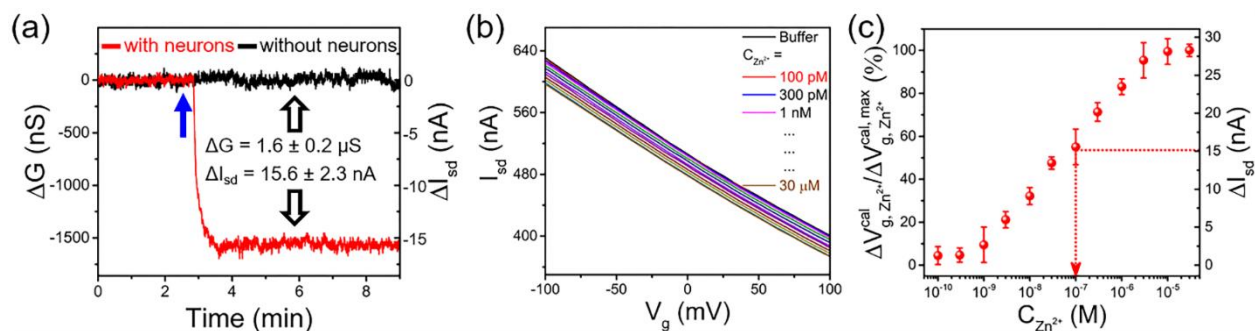
Figure S8. The responses of an Aβ/SiNW-FET to the Zn^{2+} released from AMPA-stimulated neurons. (a) The real-time conductance change (ΔG, left ordinate) and the corresponding source-drain current change (ΔI_{sd}, right ordinate) of Figure 5c were recorded with (red trace) or without (black trace) neurons under an AMPA (10 μM) stimulation (marked by a blue arrow). (b) The transfer curves (I_{sd}–V_g) of the Aβ/SiNW-FET were measured with various $C_{Zn^{2+}}$ prior to the neuron experiments in (a). (c) The $\Delta V_{g, Zn^{2+}}^{cal}$ /$\Delta V_{g, Zn^{2+}}^{cal, max}$ (left ordinate) and the corresponding ΔI_{sd} (right ordinate) of an Aβ/SiNW-FET were plotted as a function of $C_{Zn^{2+}}$ from the data points derived from (b). The $\Delta V_{g, Zn^{2+}}^{cal, max}$ represents the saturated $\Delta V_{g, Zn^{2+}}^{cal}$ measured at $C_{Zn^{2+}}$ = 50 μM. The $C_{Zn^{2+}}$ released from the stimulated neurons can be determined from the calibration curve of (c). Accordingly, the ΔI_{sd} = 15.6 ± 2.3 nA measured in (a) (i.e., Figure 5c) is converted to $C_{Zn^{2+}}$ ~100 nM released from the neurons with AMPA (10 μM) stimulation.